

## Modification of the structural properties of niobium thin films after hydrogenation

© Yu.A. Salamatov, D.I. Devyaterikov, M.V. Makarova, V.V. Matyukhov, Yu.S. Ponosov, V.V. Proglyado, E.A. Tolmacheva, E.A. Kravtsov

M.N. Mikheev Institute of Metal Physics, Ural Branch, Russian Academy of Sciences,  
620108 Yekaterinburg, Russia  
e-mail: salamatov@imp.uran.ru

Received October 25, 2024

Revised October 25, 2024

Accepted October 25, 2024

The relationships between the concentration of hydrogen absorbed in thin films of  $\text{Al}_2\text{O}_3/\text{Nb}$  type and the structural properties of these films have been established. The main research methods were X-ray diffraction and reflectometry. Structural changes after hydrogenation processes at various temperatures are analyzed. The hydrogenation conditions under which solid solutions of hydrogen in niobium and/or niobium hydrides are formed are specified. It is shown that it is possible to additionally control the concentration of hydrogen in niobium by applying a graphene layer to the film surface, obtaining an  $\text{Al}_2\text{O}_3/\text{Nb}/\text{Gr}$  type system. Being a kind of „anticatalytic layer“, graphene significantly slows down the penetration of hydrogen into the sample, which makes it possible to obtain the necessary concentrations with high accuracy.

**Keywords:** X-ray diffractometry, X-ray reflectometry, graphene, chemical vapor deposition, niobium hydrides, raman spectroscopy.

DOI: 10.61011/TP.2025.03.60864.360-24

### Introduction

The study of magnetic nanostructures with a potential to alter their magnetic ordering in a controlled fashion without the use of a magnetic field (e.g., by applying an electric field, adjusting the temperature, etc.) is one of the currently topical and rapidly developing areas in modern nanospintronics. Controlled and reversible hydrogenation is a promising method for controlling the structural and magnetic state of such nanostructures [1–4]. It has already been demonstrated in [5–7] that saturation of paramagnetic layers in Fe/Nb and Fe/V superlattices with hydrogen provides an opportunity to modify the magnetic ordering of Fe layers. In addition to the mentioned systems based on paramagnetic transition metals, superlattices based on rare-earth elements (REEs), such as Gd, Dy, and Ho, are regarded as promising candidates for hydrogenation. It is known that REEs readily absorb hydrogen from the surrounding atmosphere, and when such superlattices are kept in a hydrogen atmosphere, it will concentrate in REE layers. Varying the hydrogen pressure and hydrogenation temperature, one may alter controllably the hydrogen concentration in layers of rare-earth elements, adjusting their structural, magnetic, and electronic properties.

One important feature is that a catalytic layer on the surface of a superlattice, which facilitates the dissociation of hydrogen molecules into radicals that penetrate easily into the film, is needed for hydrogen to penetrate into REE layers. Noble metals, such as palladium or platinum, are traditionally used as these catalytic layers. They provide the possibility of hydrogenation at room temperature and low

hydrogen pressures. Among their disadvantages are the high cost and the limited temperature range of hydrogenation, since their catalytic properties deteriorate significantly at elevated temperatures due to the interdiffusion process. One rather rarely used alternative is a nickel catalytic layer. It is significantly less efficient as a catalyst, and hydrogenation requires higher temperatures, higher hydrogen pressures, and longer exposure times. We have recently studied in detail [8] the structural changes in Gd layers of Fe/Gd superlattices where hydrogenation proceeded through a catalytic nickel layer. At the same time, nickel is a ferromagnet with a Curie temperature of  $360^\circ\text{C}$ , and its presence makes the study of magnetic systems significantly more complicated.

Until now, no candidates other than those listed above have been proposed for the role of catalysts. In the present study, we examine the possibility of using niobium as a catalyst for dissociation of hydrogen molecules. Niobium is paramagnetic, which is an advantage in the context of study of magnetic systems coated with a niobium film. The process of hydrogenation of thin niobium films has been investigated for decades, but a catalytic layer of palladium was used at all times. The penetration of hydrogen into niobium layers without catalytic layers has not been studied yet. Judging by the data on hydrogenation of bulk samples of niobium, it is saturated with hydrogen fairly well, forming a solid interstitial solution (up to 10 at.% hydrogen); the solubility of hydrogen in niobium decreases with increasing temperature. At a temperature of  $360^\circ\text{C}$ , intense production of niobium hydrides  $\text{NbH}$  and  $\text{NbH}_2$  is

initiated, and significant deviations from the stoichiometric composition are observed (the fraction of hydrogen in NbH varies from 0.7 to 1). At atmospheric pressure, the intensity of reaction of niobium with molecular hydrogen remains near-zero at temperatures up to 250 °C [9,10]. The aim of the present study is to determine the optimum conditions for hydrogenation of niobium with the predominant formation of solid solution Nb–H and to establish a correlation between the structural properties of thin niobium films and the concentration of hydrogen in them.

It will be shown below that the process of saturation of niobium films with hydrogen is so intense that controlled hydrogenation requires the use of an „anticatalytic“ layer that limits the penetration of hydrogen (but does not stop it completely). Graphene is a suitable candidate in this context. Although theory [11] and experiments have demonstrated that graphene is impermeable to liquids and gases (hydrogen included), weak penetration of molecular hydrogen through graphene membranes has been reported in recent experiments [12]. This effect was attributed in [12] to the fact that graphene folds, which form naturally in the process of interaction with the substrate, act as a catalyst for dissociation of hydrogen molecules during pyrolysis. The possibility of hydrogen penetration through graphene at elevated temperatures has not been examined yet; in the present study, we demonstrate that such penetration is feasible and this effect allows one to control the hydrogenation of graphene-coated niobium films. A comparative study of hydrogen penetration into pure niobium  $\text{Al}_2\text{O}_3/\text{Nb}$  films and niobium films with a deposited graphene layer  $\text{Al}_2\text{O}_3/\text{Nb}/\text{Gr}$  was performed for this purpose.

## 1. Experimental

Niobium films 200 Å in thickness were grown on single-crystal (1102)  $\text{Al}_2\text{O}_3$  substrates by high-vacuum DC magnetron sputtering at an ULVAC setup. Sputtering was performed at room temperature; the base vacuum level in the growth chamber was  $5 \cdot 10^{-7}$  Pa, the argon pressure was 0.1 Pa, and the growth rate was  $\sim 0.5$  Å/s.

The films were cut into pieces; some of them were coated with graphene, and the remaining ones were left uncoated. A chemical vapor deposition system was used to produce graphene. Methane  $\text{CH}_4$  was the carbon source. High-purity copper foil served as a substrate and a catalyst for graphene growth. Graphene synthesis was carried out at a temperature of 1035 °C. A mixture of hydrogen and methane (the corresponding flow rates were 120  $\text{cm}^3/\text{min}$  and 5  $\text{cm}^3/\text{min}$ ) was fed into the reactor for 10 min; the pressure was  $\sim 1.3$  kPa. Following synthesis, the copper substrate was etched in a ferric chloride solution, and graphene was transferred to the niobium sample surface using a polymer film. The polymer was removed by rinsing in warm acetone. Since the potential contamination of the sample with reagent or polymer film residue should not exert any noticeable influence on hydrogen absorption

processes, these contaminants were not monitored. The transfer procedure involves repeated rinsing of the polymer film with graphene in ultrapure deionized water for removal of residual ferric chloride. A sample rinsed in acetone was dried in a chemical reactor at a temperature of 150 °C in a flow of high-purity argon. In view of this, the samples are not expected to be significantly contaminated.

The result of graphene transfer was monitored using Raman spectroscopy. Raman spectra were excited by the 532 nm (2.33 eV) line of a solid-state laser. The spectra of the  $\text{Al}_2\text{O}_3/\text{Nb}(200 \text{ \AA})/\text{Gr}$  film samples before and after hydrogenation are shown in Fig. 1. The observed  $I_G$  and  $I_{G'}$  peaks are associated with graphene transferred onto the substrate. The lack of peak  $I_D$  and intensity ratio  $I_{G'}/I_G \approx 0.86$  in the spectrum of the sample prior to hydrogenation are indicative of defect-free bilayer graphene, which was confirmed by express assessment on the „Graphene Number of Layers Calculator From  $I_D/I_G$  and  $I_{2D}/I_G$  Ratio via Raman Spectroscopy“ [13] website. Assuming that the layers in bilayer graphene are located at approximately the same distance as in graphite, one may estimate the graphene bilayer thickness at  $\sim 3.35$  Å. The second spectrum was measured in order to determine the state of graphene after hydrogenation for 5 h at 360 °C. Here, the intensity ratio is  $I_{G'}/I_G \approx 1.98$ , but the half-width of peaks also corresponds to bilayer graphene. A weak and broad  $I_D$  peak is observed; in addition, broadening and splitting of the  $I_G$  peak (compared to its initial shape) may be noted. All this points to the emergence of defects in graphene, which is likely attributable to distortions of the crystal lattice during hydrogenation.

Following the characterization of graphene deposited onto the niobium film surface, experiments on saturation of two types of systems (pure niobium  $\text{Al}_2\text{O}_3/\text{Nb}(200 \text{ \AA})$  films and graphene-coated niobium  $\text{Al}_2\text{O}_3/\text{Nb}(200 \text{ \AA})/\text{Gr}$  films) with hydrogen were performed. To avoid depletion of the working gas atmosphere, hydrogen was pumped through the reactor at a rate of 1 l/min, and atmospheric

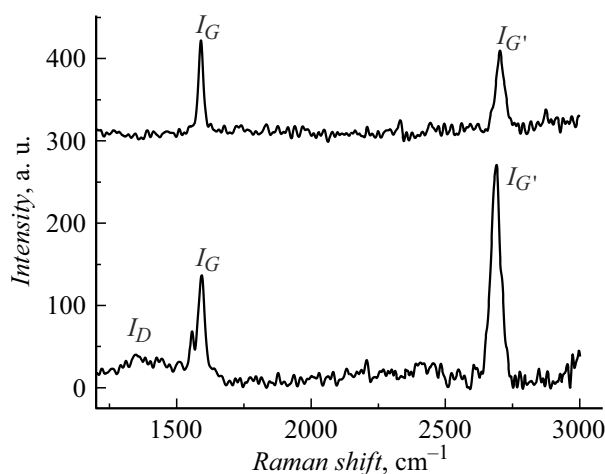


**Figure 1.** Comparison of Raman spectra of the  $\text{Al}_2\text{O}_3/\text{Nb}/\text{Gr}$  system before (top) and after hydrogenation (bottom).

**Table 1.** Experimental conditions for hydrogenation of niobium films

Samples	Process temperature, °C	Exposure time, h	Cooling conditions	Result
Al <sub>2</sub> O <sub>3</sub> //Nb(200 Å) Al <sub>2</sub> O <sub>3</sub> //Nb(200 Å)/Gr	Room	5	–	No structural changes
Al <sub>2</sub> O <sub>3</sub> //Nb(200 Å) Al <sub>2</sub> O <sub>3</sub> //Nb(200 Å)/Gr	100	5	To room temperature in argon	No structural changes
Al <sub>2</sub> O <sub>3</sub> //Nb(200 Å) Al <sub>2</sub> O <sub>3</sub> //Nb(200 Å)/Gr	150	1	To 100 °C in hydrogen, to room temperature in argon	Weak structural changes
Al <sub>2</sub> O <sub>3</sub> //Nb(200 Å)	300	1	To 100 °C in hydrogen, to room temperature in argon	Significant structural changes
Al <sub>2</sub> O <sub>3</sub> //Nb(200 Å)	360	1	To 100 °C in hydrogen, to room temperature in argon	Significant structural and chemical changes
Al <sub>2</sub> O <sub>3</sub> //Nb(200 Å) Al <sub>2</sub> O <sub>3</sub> //Nb(200 Å)/Gr	360	5	To room temperature in argon	Profound structural and chemical changes

pressure was maintained. Heating was turned off after a specified exposure time, and the samples were cooled in a hydrogen or argon atmosphere. A brief description of the experimental conditions is provided in Table 1.

The main objective was to study the temperature dependence of structural changes in hydrogenated films. An exposure time of 5 h for room temperature and 100 °C was chosen with account for the weak interaction of niobium with hydrogen at low temperatures. At elevated temperatures, the exposure was shortened to 1 h. In the last experiment, the possibility of maximum saturation of the film with hydrogen was tested, and the exposure time was increased again to 5 h, although a high temperature was maintained.

The structural changes induced by hydrogenation were studied via X-ray diffractometry and reflectometry using a PANalytical Empyrean Series 2 laboratory X-ray diffractometer. Measurements were performed in the parallel beam geometry using CoK<sub>α</sub> radiation with a wavelength of 1.79 Å. A parallel primary beam was formed by a parabolic mirror (W/Si superlattice), which also suppressed the CoK<sub>β</sub> line and the continuous bremsstrahlung spectrum. The beam height was 0.05 mm. A PIXel3D position-sensitive detector with a 2θ resolution no worse than 0.0016° was used to detect a secondary beam in diffractometry measurements. This corresponds to an absolute error of

lattice parameter determination of ~ 0.001 Å within the angular range of interest to us. In reflectometry experiments, a primary beam was shaped by a plane-parallel collimator and a planar graphite monochromator. A secondary beam was collimated by a slit with an equatorial aperture of 0.1 mm and detected by a point detector mounted in the goniometer arm.

## 2. Results and discussion

The results of X-ray diffraction measurements revealed that texture (110) forms in Al<sub>2</sub>O<sub>3</sub>//Nb(200 Å) niobium films along the normal to the sample plane. This is consistent with literature data [14]. The lattice constant of Nb and the hydrogen concentration may be estimated based on the position of the (110)Nb reflection in the diffraction patterns.

According to [15–17], anisotropic expansion of the Nb crystal lattice in the direction normal to the sample surface is observed at low hydrogen concentrations. In this case, the concentration of hydrogen in the niobium crystal lattice (in atomic percent) may be estimated as

$$c_H = \frac{N_H}{N_{Nb}} = \frac{\Delta d}{0.136 \cdot d_0}, \quad (1)$$

where  $\Delta d$  is the lattice constant variation along the normal,  $d_0$  is the lattice constant of the niobium film prior to hy-

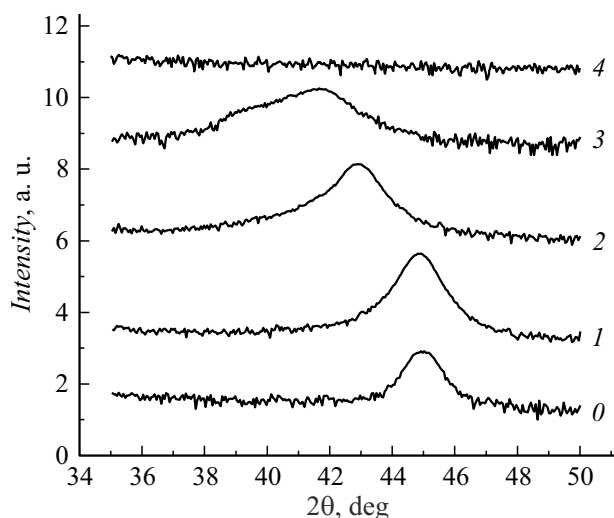


**Figure 2.** X-ray diffraction patterns of niobium films subjected to hydrogenation under various conditions: 0 — initial state before hydrogenation, 1 — at 150 °C, 2 — at 300 °C, 3 — at 360 °C, and 4 — at 360 °C for 5 h. The curves are shifted vertically for clarity. The peak is 110 Nb.

drogenation, and  $N_H$  and  $N_{Nb}$  are the numbers of hydrogen and niobium atoms, respectively. The lattice constant may differ slightly from the lattice parameter for bulk niobium due to elastic stresses induced by the interaction with the substrate, defects of the original substrate, the influence of preliminary heat treatment, etc. Therefore, the experimental lattice parameter value should be used instead of a tabular one in all cases.

At high hydrogen concentrations, the Nb lattice constant also expands in the sample plane; the following corrected formula is recommended for use in this case:

$$c_H \approx \frac{\Delta d}{0.097 \cdot d_0}. \quad (2)$$

Figure 2 presents the X-ray diffraction patterns measured for the original Nb film (without graphene) and for Nb films hydrogenated under different conditions. Since the X-ray diffraction patterns obtained after hydrogenation at room temperature and at 100 °C do not differ from the original one, they are not shown in the figure. The changes in diffraction patterns of hydrogenated samples start to manifest themselves at elevated temperatures upward of 150 °C. At 150 °C, a slight shift of the 110 Nb Bragg reflection toward smaller angles is observed, which is indicative of an increase in the crystal lattice parameter due to the introduction of hydrogen. The parameter changes by just  $(0.007 \pm 0.002) \text{ \AA}$  ( $\sim 0.2\%$ ).

Significant structural changes are observed when the hydrogenation temperature increases to 300 °C. The 110 Nb reflection shifts noticeably toward smaller angles, and a slight asymmetry is also seen. The peak shifts further toward smaller angles after 1 h of hydrogenation at 360 °C, and a second peak, which may be interpreted as a niobium

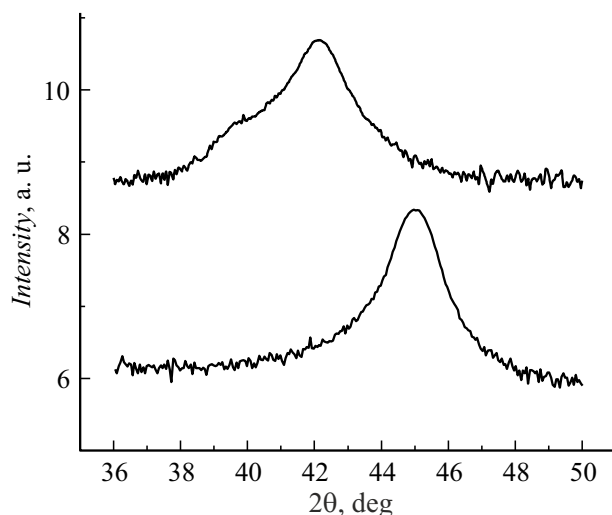


**Figure 3.** X-ray diffraction patterns of  $\text{Al}_2\text{O}_3/\text{Nb}(200 \text{ \AA})/\text{Gr}$  films before (bottom) and after hydrogenation (top). The curves are shifted vertically for clarity. The peak is (110)Nb.

**Table 2.** Concentration of hydrogen atoms in niobium film samples under different hydrogenation conditions

Sample	Hydrogenation conditions	$\Delta d/d_0$	$C_H$ , at.%
$\text{Al}_2\text{O}_3/\text{Nb}(200 \text{ \AA})$	150 °C, 1 h	0.002	1.5
$\text{Al}_2\text{O}_3/\text{Nb}(200 \text{ \AA})$	300 °C, 1 h	0.045	48
$\text{Al}_2\text{O}_3/\text{Nb}(200 \text{ \AA})$	360 °C, 1 h	0.075	78
$\text{Al}_2\text{O}_3/\text{Nb}(200 \text{ \AA})/\text{Gr}$	360 °C, 5 h	0.066	67

hydride 111  $\text{NbH}_2$  reflection, starts to emerge. Both peaks are rather low and broad, indicating significant lattice distortion. Apparently, a small amount of hydride also forms at 300 °C, which leads to the observed asymmetry. The process of saturation of the Nb film continues as the exposure time increases; the 110 Nb reflection intensity decreases with time. The hydrogen concentration in the film reaches saturation after 5 h of hydrogenation at a temperature of 360 °C, and niobium is converted completely (or almost completely) into hydride  $\text{NbH}_2$ . The lattice is distorted to such an extent that the sample becomes X-ray amorphous and all peaks vanish from the diffraction patterns.

Let us analyze the influence of graphene on the hydrogenation of Nb films. Figure 3 shows the X-ray diffraction patterns of the  $\text{Al}_2\text{O}_3/\text{Nb}(200 \text{ \AA})/\text{Gr}$  sample recorded before and after hydrogenation. The sample was hydrogenated at a temperature of 360 °C for 5 h together with an Nb film without graphene. Although the  $\text{Al}_2\text{O}_3/\text{Nb}(200 \text{ \AA})/\text{Gr}$  sample exposure time was 5 h, the hydrogen concentration was even lower than the one measured for a similar sample of pure niobium after 1 h at the same temperature. The diffraction pattern reveals a similar asymmetry (caused

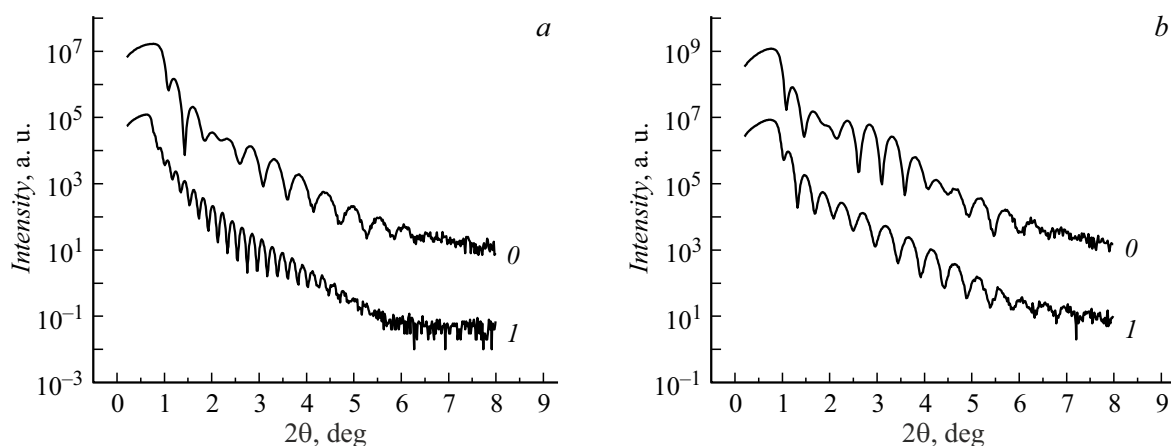


**Figure 4.** Reflectivity curves illustrating structural changes in the studied  $\text{Al}_2\text{O}_3/\text{Nb}$  (a) and  $\text{Al}_2\text{O}_3/\text{Nb}/\text{Gr}$  (b) samples. Curves 0 and 1 correspond to the initial state before hydrogenation and to the hydrogenated films, respectively. The curves are shifted vertically for clarity.

by the emergence of the (111) niobium hydride  $\text{NbH}_2$  peak); notably, it is even slightly more pronounced. This is apparently attributable to the fact that, owing to a lower concentration of hydrogen, the crystal lattice was not deformed as significantly. All this suggests that graphene is a partially permeable barrier to hydrogen penetration into niobium. Moreover, graphene has prevented significant lattice distortions, and the examined sample, in contrast to its pure niobium counterpart hydrogenated under the same conditions, did not become X-ray amorphous. These differences were also visually apparent: the niobium film without graphene lost its characteristic metallic luster and became completely transparent after hydrogenation for 5 h at  $360^\circ\text{C}$ , while the film covered with graphene did not undergo such changes.

Let us analyze the estimates of hydrogen concentration in the studied samples obtained using formulae (1) and (2) (Table 2). With the formation of hydride  $\text{NbH}_2$  taken into account, it is fair to say that the amount of hydrogen penetrating into the sample is somewhat greater than the one obtained in these calculations (hydrogen contained in the hydride compound is neglected in the given formulae). Data for the  $\text{Al}_2\text{O}_3/\text{Nb}(200 \text{ \AA})$  film kept in hydrogen for 5 h at a temperature of  $360^\circ\text{C}$  are lacking, since a diffraction peak is not found in this case.

The samples hydrogenated for 5 h were also examined by X-ray reflectometry. These samples were chosen for having the most profound structural changes. The results are presented in Fig. 4. Reflectivity curves were processed using the X'pert Reflectivity package supplied with the X-ray diffractometer. This program implements a traditional algorithm for optimizing a set of parameters (layer thickness, density, refraction index, interlayer roughness) characterizing the structure under study. These parameters are varied until an acceptable fit between the calculated and experimental reflectivity curves is achieved. It is checked at each optimization step that the parameter values do not fall outside the reasonable ranges, which are set by the operator based on a priori information regarding the sample.

In the initial state, the films have a thickness of  $205 \text{ \AA}$ , of which the upper  $30 \text{ \AA}$  correspond to the  $\text{Nb}_2\text{O}_5$  oxide. A slight film thickness non-uniformity is observed in the sample plane. Following hydrogenation, the pure niobium  $\text{Al}_2\text{O}_3/\text{Nb}(200 \text{ \AA})$  sample (Fig. 4, a) demonstrates a significant increase in thickness (up to  $470 \text{ \AA}$ ) and a noticeable reduction in density ( $5.17 \text{ g/cm}^3$  compared to  $8.57 \text{ g/cm}^3$  for pure niobium). This density is close to the reference value for niobium hydride ( $6 \text{ g/cm}^3$ ), but is lower than it due, apparently, to the high porosity of the formed layer, since the increase in thickness cannot be ascribed solely to a reduction in density. It is reasonable to assume that the sample after hydrogenation is a layer composed of crystallites smaller in size than the coherent scattering region (which leads to the vanishing of peaks in the diffraction pattern). These crystallites form a compacted nanopowder of sorts.

The situation for  $\text{Al}_2\text{O}_3/\text{Nb}(200 \text{ \AA})/\text{Gr}$  is different. The thickness and density changes in it are less significant ( $214 \text{ \AA}$ ,  $7.49 \text{ g/cm}^3$ ), but the density reduction still cannot be ascribed to just the lattice deformation due to hydrogen absorption. This verifies the conclusion from the analysis of the diffraction pattern (Fig. 4, b) that the sample contains both a solid solution of hydrogen in niobium and niobium hydride. Owing to the presence of hydride regions, the density of the sample assumes a value between the densities of pure niobium and its hydride.

## Conclusion

It was demonstrated that thin niobium films undergo a number of fairly significant structural changes in the process of hydrogenation at different temperatures and exposure times. Weak hydrogenation (up to 1 at.%) leads just to the formation of a solid solution of hydrogen in niobium. At higher hydrogen concentrations, hydrogenation is irreversible: hydrides start to form, and significant distortions are observed in the crystal lattice. Extreme

hydrogenation leads to the complete conversion of pure niobium into hydride, which is accompanied by a strong violation of crystalline ordering and the transition of the film into an X-ray amorphous state. Its thickness increases by a factor of more than 2, and its density decreases significantly.

The conditions for hydrogenation of niobium films needed to achieve the required result (formation of a solid solution and/or hydride) were determined. Graphene deposited onto the film surface acts as a barrier to penetration of hydrogen and reduces significantly its concentration inside a  $\text{Al}_2\text{O}_3/\text{Nb}/\text{Gr}$ -type sample (compared to the process of hydrogenation of a pure  $\text{Al}_2\text{O}_3/\text{Nb}$  film under the same conditions). Thus, graphene may be used for additional control over the rate of hydrogen penetration into niobium.

The obtained results are crucial for accurate analysis of structural changes occurring in the process of hydrogenation of more complex systems, such as REE/transition metal superlattices, where niobium acts as a functional layer that facilitates hydrogen penetration into the sample.

### Funding

This study was supported by grants from the Russian Science Foundation (project No. 24-12-20024) and the Sverdlovsk Oblast (project No. 2-24-OG).

### Conflict of interest

The authors declare that they have no conflict of interest.

### References

- [1] A.J. Tan, M. Huang, C.O. Avci, F. Büttner, M. Mann, W. Hu, C. Mazzoli, S. Wilkins, H.L. Tuller, G.S.D. Beach. *Nature Mater.*, **18** (1), 35 (2019). DOI: 10.1038/s41563-018-0211-5
- [2] K.Y. Lee, S. Jo, A.J. Tan, M. Huang, D. Choi, J.H. Park, H. Ji, J. Son, J. Chang, G.S.D. Beach, S. Woo. *Nano Lett.*, **20** (5), 3435 (2020). DOI: 10.1021/acs.nanolett.0c00340
- [3] G. Chen, M. Robertson, M. Hoffmann, C. Ophus, A.L.F. Cauduro, R.L. Conte, H. Ding, R. Wiesendanger, S. Blügel, A.K. Schmid, K. Liu. *Phys. Rev. X*, **11** (2), 021015 (2021). DOI: 10.1103/PhysRevX.11.021015
- [4] X. Ye, H.K. Singh, H. Zhang, H. Geßwein, M.R. Chelali, R. Witte, A. Molinari, K. Skokov, O. Gutfleisch, H. Hahn, R. Kruk. *Nat. Commun.*, **11** (1), 4849 (2020). DOI: 10.1038/s41467-020-18552-z
- [5] B. Hjörvarsson, J.A. Dura, P. Isberg, T. Watanabe, T.J. Udovic, G. Andersson, C.F. Majkrzak. *Phys. Rev. Lett.*, **79** (5), 901 (1997). DOI: 10.1103/PhysRevLett.79.901
- [6] F. Klose, C. Rehm, D. Nagengast, H. Maletta, A. Weidinger. *Phys. Rev. Lett.*, **78** (6), 1150 (1997). DOI: 10.1103/PhysRevLett.78.1150
- [7] V. Leiner, M. Ay, H. Zabel. *Phys. Rev. B*, **70** (10), 104429 (2004). DOI: 10.1103/PhysRevB.70.104429
- [8] I.A. Likhachev, I.A. Subbotin, Yu.M. Chesnokov, D.I. Devyaterikov, O.A. Kondrat'ev, A.A. Ryzhova, Yu.A. Salamатов, M.A. Milyaev, A.L. Vasil'ev, E.A. Kravtsov, E.M. Pashaev. *Phys. Metals Metallogr.*, **124** (12), 1224 (2023). DOI: 10.1134/S0031918X23602202
- [9] I.L. Knunyants, N.S. Zefirov. *Khimicheskaya entsiklopediya* (Sov. Entsikl., M., 1992) (in Russian).
- [10] A.N. Zelikman, G.A. Meerson. *Metallurgiya redkikh metallov* (Metallurgiya, M., 1973) (in Russian).
- [11] M. Miao, M.B. Nardelli, Q. Wang, Y. Liu. *Phys. Chem. Chem. Phys.*, **15** (38), 16132 (2013). DOI: 10.1039/c3cp52318g
- [12] P.Z. Sun, Q. Yang, W.J. Kuang, Y.V. Stebunov, W.Q. Xiong, J. Yu, R.R. Nair, M.I. Katsnelson, S.J. Yuan, I.V. Grigorieva, M. Lozada-Hidalgo, F.C. Wang, A.K. Geim. *Nature*, **579** (7798), 229 (2020). DOI: 10.1038/s41586-020-2070-x
- [13] *Graphene Number of Layers Calculator From ID/IG and I2D/IG Ratio via Raman Spectroscopy-InstaNANO*. URL: <https://instanano.com/all/characterization/raman/graphene-layers/> (open 13.03.2024)
- [14] D.I. Devyaterikov, V.O. Vas'kovsky, V.D. Zhaketov, E.A. Kravtsov, M.V. Makarova, V.V. Proglyado, E.A. Stepanova, V.V. Ustinov. *Phys. Metals Metallogr.*, **121**, 1127 (2020). DOI: 10.1134/S0031918X20120042
- [15] C. Rehm, H. Fritzsche, H. Maletta, F. Klose. *Phys. Rev. B*, **59** (4), 3142 (1999). DOI: 10.1103/PhysRevB.59.3142
- [16] G. Song, M. Geitz, A. Abromeit, H. Zabel. *Phys. Rev. B*, **54** (19), 14093 (1996). DOI: 10.1103/PhysRevB.54.14093
- [17] Q.M. Yang, G. Schmitz, S. Fahler, H.U. Krebs, R. Kircheim. *Phys. Rev. B*, **54** (13), 9131 (1996). DOI: 10.1103/PhysRevB.54.9131

Translated by D.Safin